10.1098/rspa.2000.0582

THE ROYAL SOCIETY

Water vapour, sonoluminescence and sonochemistry

By Brian D. Storey and Andrew J. Szeri

Department of Mechanical Engineering, University of California, Berkeley, CA 94720-1740, USA

Received 4 August 1999; revised 4 November 1999; accepted 20 January 2000

Sonoluminescence is the production of light from acoustically forced bubbles; sonochemistry is a related chemical processing technique. The two phenomena share a sensitive dependence on the liquid phase. The present work is an investigation of the fate and consequences of water vapour in the interior of strongly forced argon micro-bubbles. Due to the extreme nonlinearity of the volume oscillations, excess water vapour is trapped in the bubble during a rapid inertial collapse. Water vapour is prevented from exiting by relatively slow diffusion and non-equilibrium condensation at the bubble wall. By reducing the compression heating of the mixture and through primarily endothermic chemical reactions, the water vapour reduces the temperatures within the bubble significantly. The quantity and disposition of hydroxyl radicals produced within the bubble are studied in some detail, as this is of keen interest in sonochemistry. It was recently shown by Moss and co-workers that light emission from a sonoluminescence bubble depends sensitively on the water-vapour content. The quantity of trapped water vapour determined in the present analysis is in excellent agreement with the amount found by Moss and co-workers to match photon yields and pulse widths of recent experiments.

Keywords: sonoluminescence; sonochemistry; bubble dynamics

1. Introduction

Single-bubble sonoluminescence (SBSL) results from the intense focusing of acoustic energy by a single cavitation bubble; during the violent bubble collapse, the gas inside the bubble becomes hot enough to emit a brief flash of light (Barber *et al.* 1997). Sonochemistry is based on similar principles, where the collapses of many acoustically forced bubbles create high temperatures and pressures that promote chemical activity within or near the bubbles. A number of chemical processing applications were recently reviewed (Mason 1999; Suslick *et al.* 1999; Von Sonntag *et al.* 1999).

In the present work we study the physical and chemical consequences of water vapour on these phenomena. Water vapour has a profound effect on the peak temperatures that can be achieved during violent bubble collapses, and leads to the production of hydroxyl radicals.

During intense volume oscillations of a bubble, water is constantly evaporating and condensing, driven by dis-equilibrium between the partial pressure of water vapour inside the bubble and saturation pressure at the interface. Hence, water vapour fills

a bubble as it reaches a maximum radius. During collapse, water vapour tends to condense at the wall.

In an earlier work (Storey & Szeri (1999); henceforth referred to as S&S), we studied the diffusive segregation of noble-gas mixtures in collapsing bubbles. It was shown that the time-scale of mixture segregation due to thermal and pressure diffusion was much longer than the time-scale of the temperature peak caused by the inertial collapse and rebound. As a result, the inhomogeneous bubble composition was essentially frozen on the time-scale of the temperature peak. In the present paper, we reason along the same lines and find that the bubble motions become so rapid on collapse that the water vapour at the centre has insufficient time to escape. Therefore, excess water vapour is left behind in the bubble interior through the violent collapse.

The trapped water vapour subsequently undergoes rapid chemical reactions. These primarily endothermic reactions take up a significant amount of the focused energy, and are the basis for production of the $OH^{\bullet}$ radical that is of keen interest in sonochemistry.

Previous authors have considered these matters. Work by Kamath *et al.* (1993) separated the chemical kinetics from a Rayleigh–Plesset model to estimate the production of $OH^{\bullet}$ radicals. Gong & Hart (1998) coupled chemical reactions with a Rayleigh–Plesset equation and captured some trends observed in sonochemistry experiments. Yasui (1997*b*) accounted for chemical reactions and non-equilibrium phase change in a collapsing air bubble under SBSL conditions. Colussi *et al.* (1998) also coupled bubble motions, non-equilibrium phase change, and chemical reactions in a sonochemistry model. Sochard *et al.* (1997) modelled free-radical production in mildly forced bubbles by accounting for non-equilibrium phase change and gas–vapour inter-diffusion with a Rayleigh–Plesset model, assuming chemical equilibrium at all times.

Each of these approaches makes different simplifying assumptions, which may be valid at mild forcings. In this paper we will relax many of the usual assumptions and investigate the physics and chemistry of more strongly forced bubbles in detail. In particular, we will show that the inter-diffusion of gas and vapour is crucial to predicting the amount of $OH^{\bullet}$ produced in the bubble and the peak temperature achieved. Recently, Moss *et al.* (1999) found that inclusion of water vapour is crucial to a correct determination of photon yields and light pulse widths in SBSL; we revisit this point at the end of the paper.

In what follows, we examine the transport of water vapour into and out of the bubble. The Navier–Stokes equations of a gas mixture are coupled to a reaction mechanism to determine the fate and consequences of trapped water vapour.

2. Formulation

We shall assume that the single bubble is spherical and is composed of argon, water vapour, and reaction products ($H^{\bullet}$, H_2, $O^{\bullet}$, O_2, $OH^{\bullet}$, $HO_2^{\bullet}$, H_2O_2). For convenience, the argon is regarded as insoluble in the liquid water on the time-scale of the acoustic forcing. In S&S we showed that the flux of argon into the liquid has a negligible effect on the gas dynamics, as the total mass of argon contained in the bubble fluctuates by only *ca.* 1% over one cycle of forcing. Radiation heat transfer and light emission have negligible effects on the gas dynamics (Moss *et al.* 1999).

(*a*) *Gas dynamics*

The starting point for the study is the balance of mass, energy and momentum in spherical coordinates for an n-component gas mixture, as given in Bird *et al.* (1960). The formulation that follows differs subtly from S&S, hence we state the governing equations of the current work.

The problem is formulated in a Lagrangian way, where $r(a,t)$ is the radial coordinate at time t of a gas 'particle' that was at radial position a at $t = 0$. In the present work, the Lagrangian marker particles move with the velocity of the argon, i.e. $\partial r/\partial t = v_{\mathrm{A}}$. This reference velocity is chosen for convenience because the velocity of the bubble wall moves with the velocity of the (insoluble) argon. We note that this formulation could be modified to allow the argon to cross the moving interface.

In the present Lagrangian formulation, diffusion should be thought of relative to the background argon velocity, which may be large on collapse. Mathematically, the transform from Eulerian to Lagrangian coordinates changes the usual Eulerian material derivative as follows

$$\frac{\partial}{\partial t} + v\frac{\partial}{\partial r} \Longrightarrow \frac{\partial}{\partial t} + (v - v_{\mathrm{A}})\frac{\partial a}{\partial r}\frac{\partial}{\partial a},$$

where v is the mass average velocity.

We make the equations dimensionless using the initial values of radius R_0, density ρ_0, pressure P_0, and temperature T_0. The velocity scale, v_0, is $(P_0/\rho_0)^{1/2}$, the mass flux scale is $\rho_0 v_0$, and the internal energy and enthalpy scale is v_0^2. We make the viscosity and thermal conductivity (μ and k) dimensionless with the values at the initial state. The diffusion coefficients (D_{ij}) are made dimensionless with the average of the binary coefficient matrix, D_{avg}. Under these transformations, the mass conservation equations in dimensionless form become

$$\rho_{\mathrm{A}} J = w_{\mathrm{A},0}, \tag{2.1}$$

$$\frac{\partial w_i}{\partial t} = \frac{j_{\mathrm{A}}}{w_{\mathrm{A},0}}\frac{r^2}{a^2}\frac{\partial w_i}{\partial a} - \frac{1}{a^2}\frac{w_{\mathrm{A}}}{w_{\mathrm{A},0}}\frac{\partial r^2 j_i}{\partial a} + \frac{\Lambda_i}{\rho}, \tag{2.2}$$

where ρ is the density, w_i is the mass fraction, Λ_i is the net rate of chemical production or destruction, the subscript A denotes argon, the subscript i denotes species i, and the subscript 0 denotes the initial value. The Jacobian of the map between the reference and current configurations, J, is given by

$$J = \frac{r^2}{a^2}\frac{\partial r}{\partial a}.$$

The radial diffusive mass flux of species i with respect to the mass average velocity, j_i, is

$$j_i = -D_i^M \rho \frac{M_i}{M}\frac{1}{ReSc}\frac{\partial a}{\partial r}\left[\frac{\partial x_i}{\partial a} + \frac{Z_0 M}{\rho T M_0}(x_i - w_i)\frac{\partial P}{\partial a} + K_i^T \frac{\partial \ln(T)}{\partial a}\right],$$

where M_i is the molecular weight of species i, M is the mean molecular weight at the local conditions, x_i is the molar fraction, Z_0 is the compressibility in the initial state, K_i^T is the thermal-diffusion ratio, T is the temperature, and P is the pressure. The Schmidt number, $Sc \equiv \mu_0/\rho_0 D_{\mathrm{avg}}$, is the ratio of the diffusivity of momentum to

the diffusivity of mass; the Reynolds number is $Re \equiv \rho_0 R_0 v_0/\mu_0$. The mean diffusion coefficient, D_i^M, is a function of temperature, pressure and composition. It is defined as

$$D_i^M = \frac{1 - x_i}{\sum_{j \neq i}^{n} x_j / D_{ij}},$$

where D_{ij} is the binary diffusion coefficient between species i and j. The thermal-diffusion factor is given as

$$K_i^T = x_i \sum_{j \neq i} x_j \alpha_{ij},$$

where α_{ij} is the thermal-diffusion factor between species i and j.

The diffusive mass flux written with the mean diffusion coefficients is an approximation in the interest of computational efficiency (Gardiner 1984; Hirschfelder *et al.* 1954). The approximation is valid due to the fact that the other species (besides argon and water) are present in trace amounts. To ensure that the mass fluxes sum to zero, as is required for mass conservation, the flux of water vapour is computed as minus the sum of the fluxes of all other species, rather than in primitive form.

The balance of linear momentum written in dimensionless Lagrangian form is

$$\frac{\partial v}{\partial t} = \frac{j_{\mathrm{A}}}{w_{\mathrm{A},0}} \frac{r^2}{a^2} \frac{\partial v}{\partial a} - \frac{w_{\mathrm{A}}}{w_{\mathrm{A},0}} \frac{r^2}{a^2} \left[\frac{\partial P}{\partial a} + 3 \frac{\tau}{r} \frac{\partial r}{\partial a} + \frac{\partial \tau}{\partial a} \right], \tag{2.3}$$

where v is the mass average velocity, and τ is the deviatoric stress, given as

$$\tau = \frac{-4\mu(T, P, x_i)}{3Re} \left(\frac{\partial v}{\partial a} \frac{\partial a}{\partial r} - \frac{v}{r} \right).$$

The energy equation in these variables is

$$\frac{\partial E}{\partial t} = \frac{j_{\mathrm{A}}}{w_{\mathrm{A},0}} \frac{r^2}{a^2} \frac{\partial E}{\partial a} - \frac{w_{\mathrm{A}}}{w_{\mathrm{A},0}} \frac{1}{a^2} \frac{\partial}{\partial a} [r^2 (q + \tau v + P v)], \tag{2.4}$$

where the radial heat flux is

$$q = -\frac{C_{p0} T_0 \rho_0}{P_0} \frac{k(T, P, x_i)}{RePr} \frac{\partial T}{\partial a} \frac{\partial a}{\partial r} + \sum_{i=1}^{n} j_i H_i.$$

Here H_i is the partial molal enthalpy, and $Pr \equiv C_{p0} \mu_0 / k_0$ is the Prandtl number. We note that

$$\frac{C_{p0} T_0 \rho_0}{P_0} = \frac{\gamma}{\gamma - 1}$$

for a perfect gas, where γ is the ratio of specific heats.

(*b*) *Transport properties and equation of state*

The transport properties (μ, k, α_{ij} and D_{ij}) are calculated from equations based on the Chapman–Enskog theory using a Lennard–Jones 12–6 potential with corrections for high temperatures and densities. The individual molecular parameters are combined in an empirical way to develop effective mixture parameters for use in the single-fluid equations. These equations are given in detail in the appendix of S&S, but the essential equations are found in Hirschfelder *et al.* (1954).

There are a few minor modifications to the equations used in S&S. In the present paper, a correction is added in the combination rules for the interaction between polar and non-polar molecules. The Eucken correction is used for the thermal conductivity to account for internal degrees of freedom (Hirschfelder *et al.* 1954). Finally, the thermal-diffusion factors are computed using the approximation given by Fristrom & Monchik (1988) for computational efficiency. We stress that our previous work shows that the results are relatively insensitive to the transport properties as long as the general trends with temperature and pressure are captured.

The Soave–Redlich–Kwong equation of state (EOS) is used with combination rules for the empirical constants of the mixture (Reid *et al.* 1987). We use the polynomial data fits for ideal gas specific heats at 1 atm from Gardiner (1984) and compute departures with the EOS. While this approach may seem overly simplified compared with the EOS used in S&S, a similar EOS for water and its reaction products that allows us to account for finite-rate chemistry is not available. It was found in S&S, and again in the present work, that the EOS has no impact on the basic physics of the problem and only modifies the final quantitative answers.

(*c*) *Motion and energy transport in the liquid*

Rather than solve the Navier–Stokes equations governing the motion of the liquid, we assume that a Rayleigh–Plesset-type equation for the bubble radius is valid. The Rayleigh–Plesset equation is an ordinary differential equation for the bubble radius, which is coupled with the gas dynamics of the interior through the pressure and stress at the bubble wall. The form of the equation we use is similar to the one derived by Prosperetti & Lezzi (1986), differing only in that the present work accounts for the extra velocity at the interface due to evaporation or condensation. The effect of evaporation–condensation on the Rayleigh–Plesset equation is very small, but the effect is included for consistency. The resulting equation is similar to ones derived by Yasui (1997*a*) and by Fujikawa & Teruaki (1980).

Rather than solve the full energy equation in the liquid, we solve the boundary-layer form, as described in detail by Fyrillas & Szeri (1994). The boundary-layer assumption reduces the energy equation to the linear diffusion equation in Lagrangian boundary-layer coordinates. This approximation for the energy equation was used in Vuong & Szeri (1996) and in S&S.

(*d*) *Evaporation and condensation*

The equation derived from kinetic theory given in Carey (1992) is used to compute the rate of evaporation and condensation at the bubble surface. This is written in dimensionless variables as

$$\left.\begin{aligned} \dot{m}''_{\mathrm{kin}} &= \sqrt{\frac{M_{\mathrm{H_2O}} Z_0}{2\pi M_0}}\left(\frac{\Gamma P_{\mathrm{H_2O}}}{\sqrt{T_{\mathrm{int}}}} - \frac{P_{\mathrm{sat}}}{\sqrt{T_{\mathrm{int}}}}\right), \\ \dot{m}''_{\mathrm{act}} &= \sigma \dot{m}''_{\mathrm{kin}}. \end{aligned}\right\} \tag{2.5}$$

Here, $\dot{m}''_{\mathrm{kin}}$ is the rate at which water molecules hit the interface (from kinetic theory), σ is the accommodation coefficient (sticking probability), $\dot{m}''_{\mathrm{act}}$ is the rate at which water molecules hit the interface and undergo phase change, $P_{\mathrm{H_2O}}$ is the partial

pressure of water, $P_{\rm sat}$ is the saturation pressure at the temperature of the interface $T_{\rm int}$, M_0 is the initial molecular mass of the bubble contents. Γ is a correction for bulk motion to the interface and remains close to one for low mass transfer. We emphasize that this equation is only valid for reasonable temperatures and pressures, and not at the extreme conditions found during a bubble collapse. As we argue below, the evaporation condition is of vanishing consequence during the terminal stages of bubble collapse when (2.5) loses validity.

There is some discord in measurements of the accommodation coefficient. The value we use, $\sigma = 0.4$, is consistent with that used by Yasui (1997*a*) (developed from molecular dynamics simulations) and those recommended by Eames *et al.* (1997). The sensitivity of the results to the accommodation coefficient will be considered later.

(*e*) *Chemical kinetics*

Chemical kinetics, described by the reaction mechanism, determines the production and destruction of the different species. The reaction mechanism that we use is described in Maas & Warnatz (1988). The mechanism includes 19 forward and reverse elementary reactions and nine species (Ar, $H^{\bullet}$, H_2, $O^{\bullet}$, O_2, $OH^{\bullet}$, $HO_2^{\bullet}$, H_2O_2). Argon only enters the mechanism as a third body.

The net rate of progress of each elementary reaction is the difference in the forward and reverse rate of progress. The forward (reverse) rate of progress is given as the product of the reaction rate and the concentrations of all species on the reactant (product) side of the equation. The change in concentration of species i with time is the sum of the net rate of progress of each elementary reaction that contains species i. The details can be found in several texts (e.g. Gardiner 1984). In the present formulation, the chemical kinetics lead to the net chemical production or destruction term, Λ_i, in (2.2).

The reaction rates are given empirically with the reaction mechanism. The Lindemann form is used to take into account the pressure fall-off in some of the three-body reactions (Gardiner 1984). The high-pressure limit of the reaction rates for available reactions were taken from Bowman *et al.* (1999).

The elevated pressure in the bubble upon collapse accelerates the *rate of progress* of the reactions, and alters the equilibrium state to which the reactions tend, so that for a given temperature there is less dissociation at higher pressures. This change in equilibrium state with pressure is accounted for in the reaction mechanism, because forward and reverse reaction rates are related through the equilibrium constant. There is considerable uncertainty in the *reaction rates* at the high pressures we shall encounter. The mechanism and reaction rates we use seem to be the best ones presently available.

The reaction mechanism does not include ionization reactions. The onset of ionization is delayed due to the high pressure. The degree of ionization at the conditions we report is quite low as estimated by the Saha equation. Moss *et al.* (1997) put forth the criterion that the onset of ionization in a dense gas is at one-quarter of the ionization potential; in the present case, this temperature is *ca.* 30 000 K. The results we present are consistent with neglecting ionization based on either of these criteria.

(*f*) *Mass transfer to the liquid*

One of the most difficult quantities to determine accurately is the rate of transport of radical species into the liquid. While general convection–diffusion–reaction equations can be written for each species dissolved in the liquid, this approach involves many unknowns. For example, data on the solubility of $OH^{\bullet}$ radicals in liquid water vary by two orders of magnitude (Sander 1998). We know of no solubility data for $H^{\bullet}$ or $O^{\bullet}$. Moreover, there is the possibility of heterogeneous surface reactions (Von Sonntag *et al.* 1999), which are poorly understood, especially at the time of collapse when the liquid very near the bubble interface is supercritical.

To avoid these uncertainties we take a very simple approach. To determine the rate of radical invasion into the liquid approximately, we introduce the uptake coefficient, Θ,

$$\Theta = \frac{N_{\mathrm{in}} - N_{\mathrm{out}}}{N_{\mathrm{coll}}}, \tag{2.6}$$

where N_{in} is the number of molecules invading the liquid, N_{out} is the number of molecules ejected from the liquid, and N_{coll} is the number of molecules colliding with the surface (from kinetic theory). This view of mass transfer is oversimplified; one can easily see that Θ is not an intrinsic quantity (Takami *et al.* 1998; Chameides 1984).

This approach has, nevertheless, been used to determine the absorption of radical species onto liquid and solid surfaces. The uptake coefficients have been measured for some of the species in our system over aqueous surfaces (Takami *et al.* 1998; Hanson *et al.* 1992). We shall study the influence of uptake coefficient on the results of our calculations below.

(*g*) *Numerical method*

The same Chebyshev collocation method is used that was described in detail in S&S. The variables in the gas are approximated by expansions in Chebyshev polynomials in the argon Lagrangian coordinate, a. The temperature in the liquid is approximated with an expansion in rational Chebyshev polynomials. The equations in the gas evolve with a straightforward explicit predictor–corrector scheme. We use standard operator splitting (Press *et al.* 1988) to solve the chemical kinetics equations separately, with a semi-implicit method to avoid time-step restrictions caused by the stiffness of these equations. The energy equation in the liquid is integrated in time with a fully implicit method to avoid time-step restrictions associated with the close spacing of grid points near the bubble wall. As an error check, global balances of mass and energy are monitored; imbalances always remain below a fraction of a per cent.

3. Results and discussion

We begin by presenting detailed results of one particular configuration. Due to the complexity of the problem, we shall attempt to present the results in a systematic way in order to demonstrate the importance of certain phenomena. The cases to be investigated are as follows.

Table 1. *Summary of the different cases investigated in detail*

(In all cases the bubble is a 4.5 μm radius argon bubble in water at 298 K acoustically forced with a 1.2 bar pressure amplitude at 26.5 kHz.)

case	phase change	chemistry	$OH^{\bullet}$ uptake	R_{max}/R_{min} (μm)	T_{max} (K)
I	no	no	0.0	28.0/0.80	20 900
II	yes	no	0.0	31.3/0.70	9 700
III	yes	yes	0.0	31.7/0.65	7 000
IV(a)	yes	yes	0.001	31.7/0.65	7 000
IV(b)	yes	yes	0.01	31.7/0.65	7 000

Case I: *no* water vapour allowed in the bubble.

Case II: water vapour allowed to evaporate and condense but *no* chemical reactions.

Case III: water vapour and chemical reactions but *no* mass transfer across the bubble interface.

Cases IV(a) and IV(b): mass transfer of $OH^{\bullet}$ across the bubble interface at different uptake coefficients.

In all cases the bubble is a 4.5 μm-radius argon bubble in 298 K water acoustically forced with a 1.2 bar pressure amplitude at 26.5 kHz. These cases are summarized in table 1. With respect to SBSL, this bubble was found to be stable to mass exchange and shape changes, though would have minimal light emission (Hilgenfeldt *et al.* 1996; Wu & Roberts 1998*a*, *b*). We describe the results for more strongly forced bubbles below. The data we obtain are for steady-state oscillations, i.e. after the decay of initial transients. After presenting the details of these cases, we consider variations in the parameters to illustrate interesting trends.

(*a*) *Excess water is trapped by the rapid collapse*

We shall now argue that significant amounts of water vapour become trapped in the interior of the bubble when it collapses violently. Water is trapped in the interior because the bubble motions become so rapid that the vapour near the centre has insufficient time to diffuse to the bubble wall. Non-equilibrium phase change also plays a significant role in the amount of water that is trapped. All results in this subsection apply to case II; this case allows one to focus on the dynamics of evaporation, condensation and diffusion of water inside the bubble without the complication of chemical reactions.

In figure 1, we show the radial history of the bubble over one cycle of the acoustic forcing in case II. The essential features of the bubble dynamics for cases I and II are the same, but the inclusion of water vapour increases the maximum radius and delays the collapse. The difference is to be expected because case I has no vapour pressure. The compression ratio (R_{max}/R_{min}) for cases I and II is 35 and 44, respectively. The compression ratio is an approximate way of separating out differences in the results due to differences in the bubble dynamics. Typically, a higher compression ratio leads to more compression heating and higher temperatures, if all else is equal. We return to this point later.

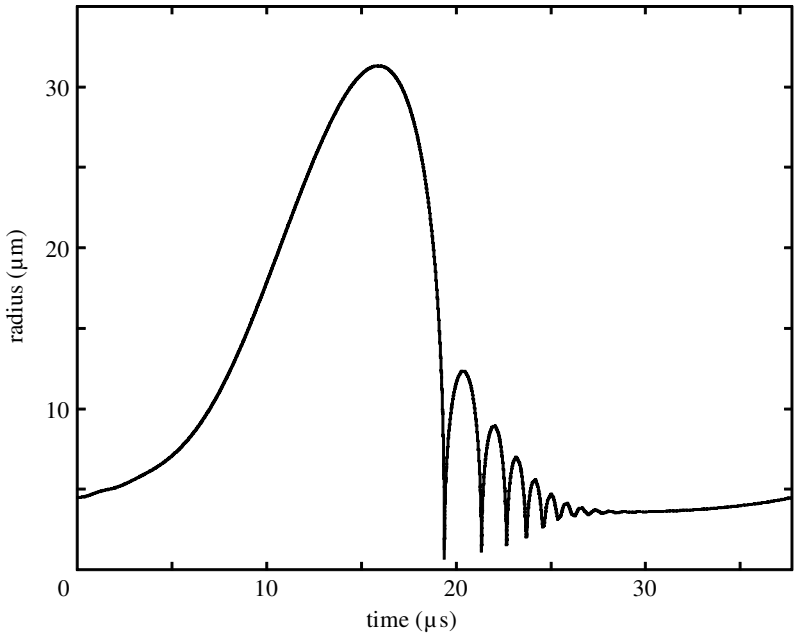

Figure 1. Radius of the bubble versus time over one cycle of acoustic forcing in case II. The essential features for cases I, II, III and IV are the same.

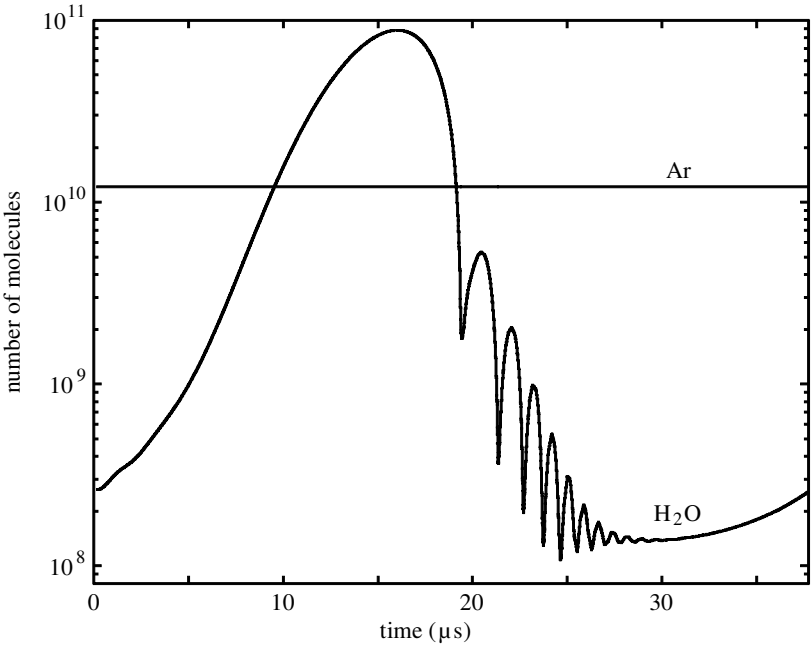

Figure 2. Total number of water-vapour molecules contained in the bubble versus time over one cycle of acoustic forcing in case II. Note that water comprises *ca.* 14% of the bubble contents at the end of the main collapse.

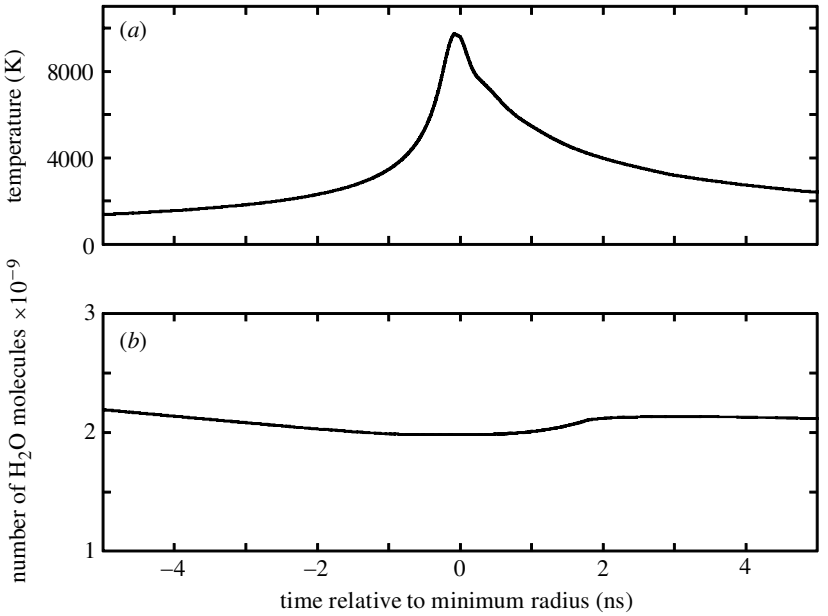

Figure 3. Temperature (a) and total number of water molecules contained in the bubble (b) versus time around the point of minimum radius (time = 0) in case II. The temperature undergoes order-of-magnitude changes on this time-scale, while the total number of water molecules changes very little.

In figure 2, we show the total number of H_2O molecules contained within the bubble over the acoustic cycle (case II). A large amount of water evaporates into the bubble during the main expansion when the pressure is low. Water condenses on the bubble wall during the collapse as the gas pressure increases. There is significant water vapour in the bubble at the main collapse: *ca.* 14% (molar basis) of the total bubble contents is water vapour. If the interface were at equilibrium and the speed of mass diffusion were infinite, there would be a negligible amount of water in the bubble on collapse.

In figure 3, we show the temperature history of the centre and the total number of water molecules in the bubble around the time of minimum radius (time = 0) in case II. Over the 10 ns time-scale, the total amount of water vapour contained in the bubble is nearly constant, whereas the temperature changes by an order of magnitude. This recalls S&S, in which it was shown that evolving mixture compositions were essentially frozen on the time-scale of the temperature peak.

The temperature peak may be related to the light emission. The equation for optical power given by Moss *et al.* (1999), with a constant opacity, provides an easy estimate for the optical power output as a function of time. For case II, this estimate gives a light emission pulse width (FWHM) of 350 ps, which is much shorter than the *ca.* 2000 ps temperature peak. This optical-pulse-width estimate would be somewhat shortened if the temperature dependence of the opacity were taken into account. The peak optical power is *ca.* 0.1 mW, although this number is very sensitive to the opacity. Typical stable SBSL experiments (at higher forcings than the present case) yield light emission of the order of milliwatts per flash (Gaitan *et al.* 1996; Hiller *et al.* 1992).

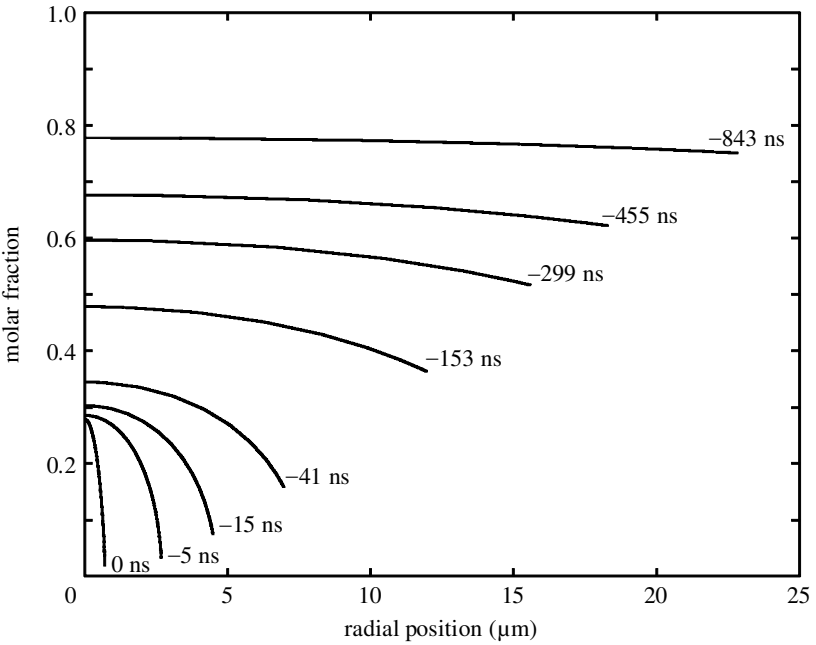

Figure 4. Molar fraction of water vapour versus radius for selected times prior to the moment of minimum radius (time = 0) in case II. Note the development of the non-uniform composition as the collapse accelerates toward minimum radius. In the last 15 ns before minimum radius, the composition changes by only a few per cent when viewed in the Lagrangian frame instead.

There are two mechanisms that determine the excess vapour left behind at the collapse: finite-rate mass diffusion and non-equilibrium phase change. We examine each mechanism and their interaction in turn.

(i) *Role of diffusion*

The first reason for excess water vapour remaining during the collapse is the rapid bubble collapse overwhelming slow mass diffusion: this was extensively discussed in S&S. In S&S it was shown that there is a competition between two important time-scales: the dynamic time-scale of the bubble motions and the mass diffusion time-scale. These are given explicitly in dimensionless terms as

$$\tau_{\mathrm{dyn}} = R/\dot{R},$$
$$\tau_{\mathrm{dif}} = ReSc\frac{R^2}{D^{\mathrm{M}}_{\mathrm{H_2O}}} \approx ReSc\frac{1}{R\sqrt{T}}.$$

In the latter, we made use of the fact that the diffusion coefficient of water vapour in the gas mixture, $D^{\mathrm{M}}_{\mathrm{H_2O}}$, scales as $R^3\sqrt{T}$.

The time-scales argument is clarified upon examination of figure 4, which shows the evolving bubble composition as a function of radius at selected times before the time of minimum radius (case II). In the early part of the collapse, the dynamic time-scale is longer than the diffusion time-scale, $\tau_{\mathrm{dyn}} \gg \tau_{\mathrm{dif}}$; this results in a uniform composition of the bubble (upper curves in figure 4). As the bubble accelerates into

the collapse, $\tau_{\rm dyn} \sim \tau_{\rm dif}$ and the decrease in water fraction at the centre begins to lag, the decrease in water fraction at the wall (middle curves of figure 4). Further into the collapse, $\tau_{\rm dyn} \ll \tau_{\rm dif}$ and the water vapour cannot diffuse to the bubble wall on the time-scale of the rapid collapse. This slow diffusion results in a nearly fixed distribution of water vapour (three lowest curves of figure 4).

While the three lowest curves in figure 4 look quite different in this Eulerian representation, they differ by only a few per cent when viewed in the Lagrangian representation (not shown). The curve at -15 ns is from a time when $R = R_0$, and the temperature at the centre is *ca.* 750 K. The curve at 0 ns is from the time of minimum radius ($0.15R_0$), when the temperature at the centre is 9700 K. Consistent with figure 3, over times when there are drastic changes in the bubble radius and temperature, the composition of the bubble is almost a material field.

(ii) *Role of non-equilibrium phase change*

Non-equilibrium phase change is the second mechanism by which vapour is trapped in the bubble interior during the collapse. By adjusting the accommodation coefficient, one has control over the time-scale for the partial pressure of the water vapour to come to equilibrium with the saturation pressure at the interface. The dimensionless condensation time-scale is

$$\tau_{\rm cond} = \frac{R}{\sigma}\sqrt{\frac{2\pi M_{\rm H_2O}}{9M_0T_{\rm int}}}.$$

When $\tau_{\rm dyn} \gg \tau_{\rm cond}$, the condensation is in quasi-equilibrium with respect to the bubble motions. If $\tau_{\rm dyn} \ll \tau_{\rm cond}$, then the bubble collapse is so rapid that no mass can escape the bubble on the time-scale of the collapse.

(iii) *Interaction of the two mechanisms*

It is the competition between the time-scales for mass diffusion, condensation and bubble dynamics that determines which mechanism traps water vapour in the bubble. Once $\tau_{\rm dyn} \ll \tau_{\rm dif}$ or $\tau_{\rm dyn} \ll \tau_{\rm cond}$, the total amount of water vapour in the bubble is fixed. Only one of these conditions needs to be met for vapour to be trapped in the bubble. Both mechanisms can, however, participate to determine the quantity of trapped vapour.

During the bubble collapse, the condition $\tau_{\rm dyn} \ll \tau_{\rm dif}$ is reached well before $\tau_{\rm dyn} \ll \tau_{\rm cond}$ in case II. Therefore, in this case (as well as the others presented herein), it is the slow mass diffusion that is responsible for trapping vapour in the bubble.

For cases where slow mass diffusion traps the vapour, non-equilibrium phase change helps to determine the amount trapped. The accommodation coefficient represents a resistance to condensation at the interface during collapse of the bubble. A lower value of accommodation coefficient provides more resistance to phase change, clearly increasing the mass of water retained in the bubble at any time during the collapse. The importance of the non-equilibrium phase change can be estimated by comparing $\tau_{\rm dyn}$ with $\tau_{\rm cond}$ at the time that $\tau_{\rm dyn} = \tau_{\rm dif}$. The closer $\tau_{\rm dyn}$ is to $\tau_{\rm cond}$, the more important non-equilibrium phase change is in determining the amount of water trapped.

Colussi *et al.* (1998) developed a model including chemical reactions in a collapsing bubble using an accommodation coefficient of $\sigma = 0.001$, but did not take into

account the finite rate of mass diffusion. The low value of σ, which works to trap significant water vapour at collapse, was necessary for their model to be consistent with experimental sonochemistry data. When such a low value for σ is used, the condition $\tau_{\mathrm{dyn}} \ll \tau_{\mathrm{cond}}$ is reached well before $\tau_{\mathrm{dyn}} \ll \tau_{\mathrm{dif}}$ (the opposite of our case). Such a low accommodation coefficient works to trap significant amounts of water vapour in the bubble, but in this case the hindered flux at the interface eliminates mass transfer out of the bubble while the distribution of water vapour within is essentially uniform. In the present work, we argue that the significant amounts of water vapour trapped in the bubble are a consequence of slow diffusion as well as non-equilibrium phase change.

The temperature of the interface exceeds the critical point for a very brief time (from −340 ps to 1800 ps relative to the time of minimum radius). For the conditions we explored, the maximum thickness of the supercritical region is quite thin, less than 1% of the bubble radius, i.e. *ca.* 10 nm. We neglect any changes in the liquid equation of state and transport properties when the interface exceeds the critical temperature. This assumption is justified based on the thinness of the region, and the fact that the critical temperature is reached very late in the collapse. Any disturbances caused by the supercritical interface have insufficient time to propagate into the bubble interior on the main collapse. Although the evaporation equation is invalid for these short times, the total mass added to the bubble is negligible, regardless of the magnitude of evaporative mass flux. The issue of the super-critical interface may require future improvements, but is beyond the scope of the present work.

As a final note, both thermal and pressure diffusion also play a role in determining the distribution of water vapour during the collapse. In the argon–water system, the thermal-diffusion coefficient is small and the molecules are of similar size, hence pressure diffusion is quite weak. Little difference is seen in calculations with and without these other forms of mass diffusion. In a helium or xenon bubble in water, thermal and pressure diffusion are more pronounced and can cause a 10–15% difference in the amount of trapped water vapour. In the interest of brevity, we will not discuss these results further here.

(*b*) *Gas-phase chemical reactions break apart* H_2O *and reduce the temperature*

Now we turn to an investigation of what transpires when chemical reactions are taken into account (case III). We shall show that there is significant time for reactions to occur, i.e. the time-scale for chemical reaction is similar to that of the bubble collapse. The primarily endothermic reactions absorb a significant amount of energy and further reduce the peak temperatures from cases I and II. The distribution of species produced in the bubble is determined by diffusive transport of water vapour prior to the collapse and heat transfer out of the bubble during the collapse. The steep temperature gradient at the wall confines the bulk of the chemical reactions to the bubble interior.

(i) *Consequences of chemistry*

The overall bubble dynamics of cases II and III are essentially the same with a compression ratio of 49 in case III (slightly higher than case II). A convenient point of departure is to compare the temperature histories of the bubble centre around the main collapse for the three cases we have considered (see figure 5). The inclusion

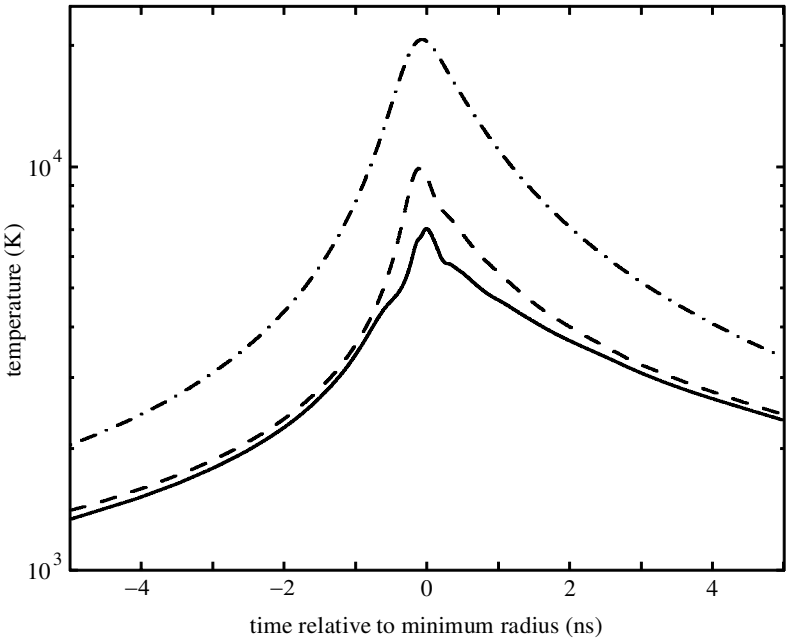

Figure 5. Temperature history of the centre of the bubble around the time of minimum radius ($t = 0$) in cases I, II and III. Note the reduction in temperature from case I (– · – · –) to case II (– – –) as water is allowed to enter the bubble. The chemical reactions added in case III (——) further reduce the temperatures.

of water vapour (case II) significantly reduces the peak temperature from case I. The decrease in temperature is due mainly to the decrease in the ratio of specific heats of the mixture, which reduces the compression heating. Upon comparison of cases II and III, one observes that the chemical reactions further reduce the peak temperature due to the endothermic decomposition of the water vapour. The centre temperature histories of cases II and III are nearly identical below 4000 K.

It is important to understand that the temperature differences in these three cases are not due to subtle differences in bubble dynamics. The compression ratio ($R_{\max}/R_{\min}$) of the three cases increases from case I to case II to case III, whereas the temperature *decreases* in this order. This decrease in temperature occurs despite the fact that a higher compression ratio will lead to more compression heating in the bubble collapse, all other things being equal. In all these cases there are no shocks inside the bubble. Shocks will be considered in § 3 *e*.

In figure 6, we show the history of the total number of molecules of the different species as a function of time on the same time-scale as in figure 5. The lowest curve is the total amount of water vapour only. The next curve is the total amount of water vapour plus the total amount of H_2. Each curve represents the addition of one species, as labelled, until the uppermost curve denotes everything but argon. We do not label $HO_2^{\bullet}$ and H_2O_2 as they appear only in trace amounts. One observes which species are most abundant during the time of the main collapse. Note there is a relatively large amount of undissociated water considering the elevated temperatures. This is primarily a consequence of the high pressure suppressing the dissociation of H_2O.

From figures 5 and 6 one observes that the onset of significant chemical activity in

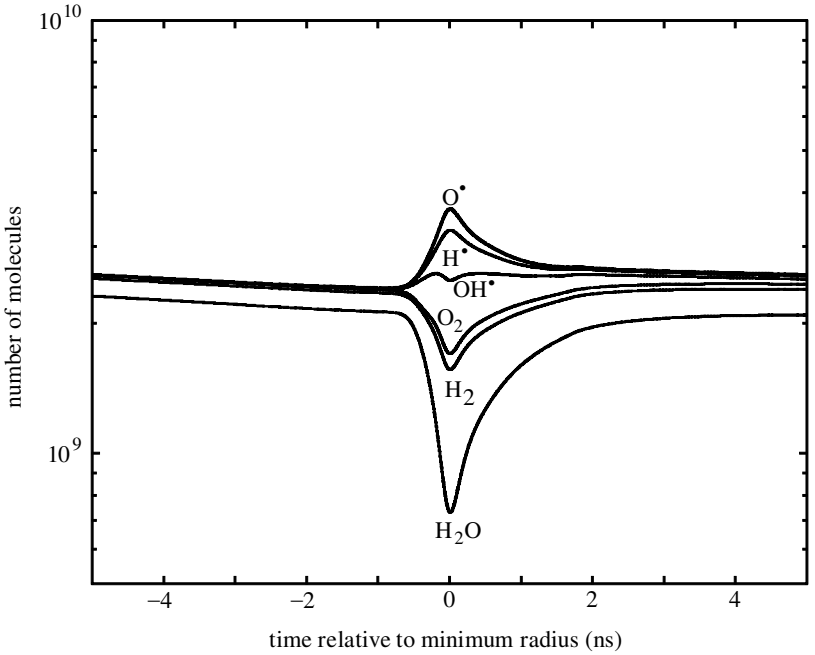

Figure 6. Cumulative number of molecules of each species in case III. The lowest curve is the total number of water molecules, the next curve is total water + H_2, and so on. H_2O_2 and $HO_2^{\bullet}$ are neglected in this plot as they appear in trace amounts.

the bubble corresponds to a centre temperature of *ca.* 4000 K. Therefore, the reduced temperature of case III shown in figure 5 can be attributed to the endothermic chemical reactions. Although the bubble dynamics are quite rapid, the chemical reactions keep pace, as is shown by the similar time-scales of the changing quantities in figures 5 and 6. The rapid rate at which the reactions progress is due to the very high density. Recall that the rate of progress of each reaction is directly related to the species concentration (mol cm^{-3}).

(ii) *Dynamics and distribution of* $OH^{\bullet}$ *production*

In sonochemistry applications, the invasion of $OH^{\bullet}$ radicals into the liquid is thought to be responsible for much of the complex and useful chemistry that occurs. Therefore, we shall focus on the behaviour of this species in particular. In figure 7, we plot the total number of $OH^{\bullet}$ molecules contained in the bubble on two time-scales: over one acoustic cycle in figure 7*a*; and around the time of collapse in figure 7*b*. The initial concentrations of all species were selected so that the chemical production and destruction balanced in one acoustic cycle. The main collapse is associated with a rapid creation of $OH^{\bullet}$ once the temperature exceeds 4000 K.

Upon rebound, the bubble rapidly cools and the $OH^{\bullet}$ and other products tend to recombine back into H_2O. These recombination reactions proceed more slowly than the dissociation reactions upon collapse. The result is that the bubble is left with a super-equilibrium amount of $OH^{\bullet}$ after it has cooled to ambient temperature. This super-equilibrium $OH^{\bullet}$ then slowly decays through the rest of the cycle with brief spurts of production and destruction at each of the after-bounces.

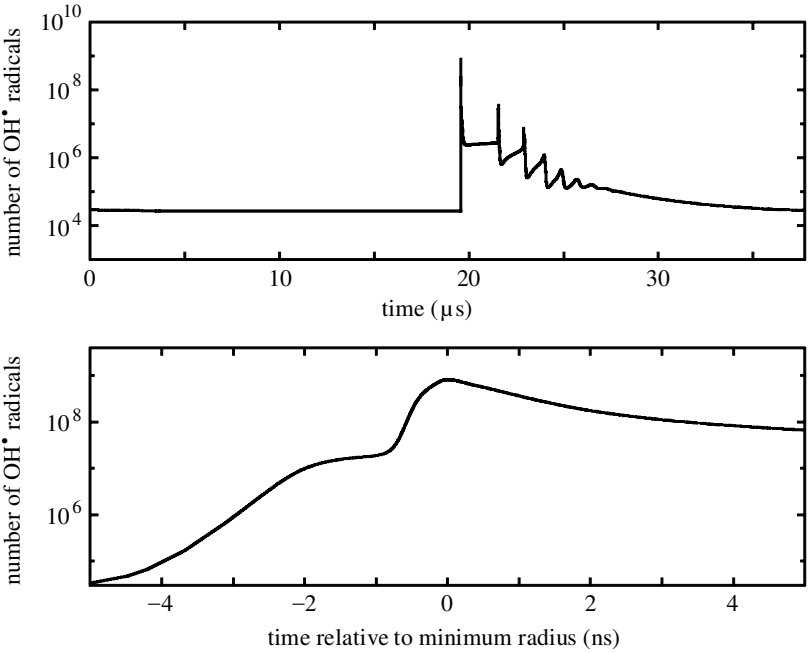

Figure 7. Total number of $OH^{\bullet}$ molecules contained in the bubble versus time over one acoustic cycle (*a*) and around the time of minimum radius (*b*) in case III. The first sharp peak in (*a*) is expanded in (*b*). Subsequent peaks in (*a*) correspond to local radius minima in the bubble dynamics. The initial amounts of $OH^{\bullet}$ and all the other species were chosen for no net species production or destruction over an acoustic cycle.

The distribution of $OH^{\bullet}$ in the bubble is characterized by a fairly uniform concentration through much of the bubble interior and a very sharp gradient near the wall. This sharp gradient is a result of heat transfer during the collapse. During compression, conduction between the hot interior and the cool wall sets up a thin temperature boundary layer. This boundary layer confines the chemical reactions to the interior, away from the interface. The cooler wall leads to a much lower concentration of $OH^{\bullet}$ at the interface than in the centre at the time of the main collapse. In figure 8 we show the molar concentration history of $OH^{\bullet}$ at the centre and at the interface. When the bubble is at minimum radius and the $OH^{\bullet}$ concentration at the centre is at its maximum, the concentration at the wall is three orders of magnitude lower.

Because the chemistry time-scale is much faster than the diffusion time-scale, $OH^{\bullet}$ is produced where water vapour was trapped at high enough temperature. The liquid interface is insulated from the high concentration of $OH^{\bullet}$ generated deep inside in the bubble. The only $OH^{\bullet}$ produced at the centre that reaches the bubble interface is the slowly decaying super-equilibrium $OH^{\bullet}$ that is left inside the bubble on re-expansion.

(*c*) $OH^{\bullet}$ *uptake by the liquid does not influence the bubble interior*

The inclusion of liquid uptake of $OH^{\bullet}$ (case IV) adds further complications; we now try to illuminate some of the main qualitative features. We shall argue that $OH^{\bullet}$ uptake has little effect on the gas dynamics and chemical production.

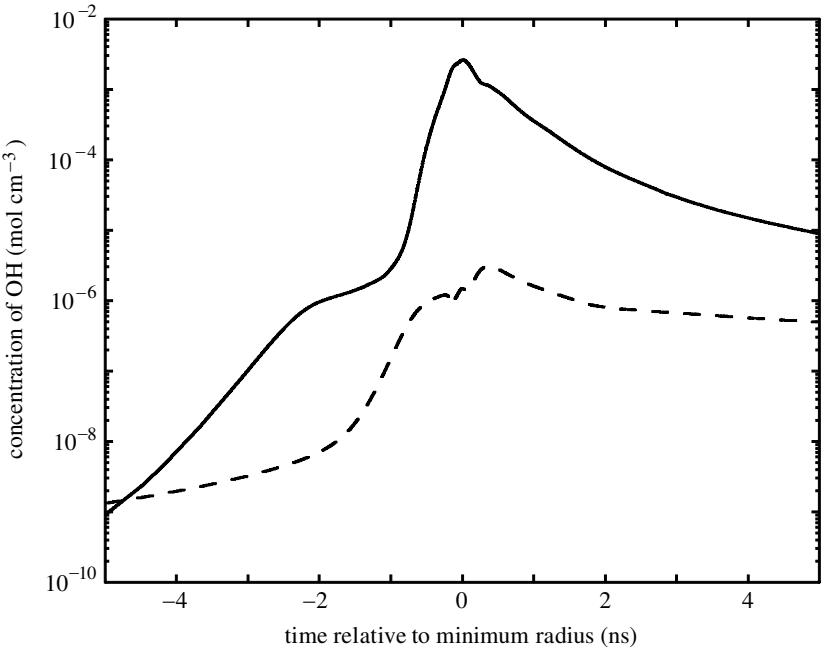

Figure 8. Molar concentration of OH$^{\bullet}$ at the centre (——) and the interface (– – –) versus time around the point of minimum radius. Note that the concentration at the centre is about three orders of magnitude greater than at the interface at the point of minimum radius.

Due to differing ideas on the proper value of the uptake coefficient, the values are set at $\Theta = 0.001$ and $\Theta = 0.01$ (cases IV(a) and IV(b)) consistent with the work of others to which we made reference earlier. The bubble dynamics and temperature profiles for cases IV(a) and IV(b) are indistinguishable from those for case III. In figure 9 we show the total number of OH$^{\bullet}$ molecules in the bubble versus time on two different scales for cases III, IV(a) and IV(b). The history for one acoustic cycle is plotted in figure 9*a*, and the history concentrated at the main collapse is plotted in figure 9*b*.

In the main expansion when the bubble is cool, the OH$^{\bullet}$ resident in the bubble will invade the liquid, as can be seen by the decrease in the amount of OH$^{\bullet}$ at the end of the long expansion as the uptake increases. When the bubble collapses, the chemical production of OH$^{\bullet}$ from recently evaporated water rapidly overwhelms the OH$^{\bullet}$ uptake by the liquid. As the bubble proceeds into the collapse, the curves of total OH$^{\bullet}$ content for different uptakes become indistinguishable. The total amount of OH$^{\bullet}$ in the bubble is dominated by the amount created in the interior, away from the wall. The total amount of OH$^{\bullet}$ lost to the liquid during a collapse is only a fraction of the amount contained in the bubble. Hence, the peak amount of OH$^{\bullet}$ in the bubble during the collapse is insensitive to the uptake coefficient of OH$^{\bullet}$. Similar statements apply to uptake of other species.

In figure 10 we show, for the purposes of qualitative discussion, the total mass of OH$^{\bullet}$ exiting the bubble in cases IV(a) and IV(b). While the OH$^{\bullet}$ uptake coefficient does not influence the total amount of OH$^{\bullet}$ contained in the bubble at the main collapse, there are large differences in the amount invading the liquid over

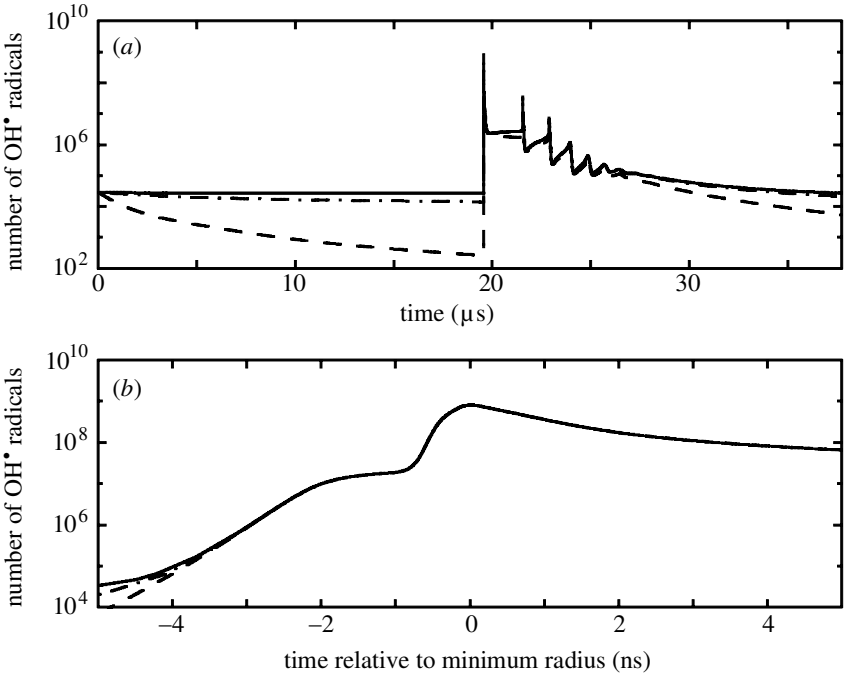

Figure 9. Comparison of total amount number of $OH^{\bullet}$ molecules in the bubble versus time over one acoustic cycle (*a*), and focused around the time of minimum radius (*b*) in cases III (——), IV(a) (– · – · –) and IV(b) (– – –). The uptake of $OH^{\bullet}$ plays a role during the slow expansions when the resident amount of $OH^{\bullet}$ left in the bubble is well above chemical equilibrium. At the collapse, $OH^{\bullet}$ uptake does not influence the total amount of $OH^{\bullet}$ production.

a cycle. Much of the $OH^{\bullet}$ uptake occurs during the main collapse and the subsequent re-expansion when the concentration of $OH^{\bullet}$ at the wall is at its maximum (see figure 8). Further uptake occurs throughout the cycle at each of the after-bounces.

(*d*) *Inclusion of water vapour alters the effect of increased forcing*

Next we shall compare the results of cases I, II and III with all parameters fixed except for the acoustic pressure amplitude, which varies between 1.0 and 1.3 bar. We that note this is experimentally awkward for SBSL, because pressure amplitude and ambient radius are *dependent* quantities through the mass exchange equilibrium of rectified diffusion (Hilgenfeldt *et al.* 1996). The way we present these results is nonetheless useful, as it demonstrates the importance of water vapour in the understanding of sonoluminescence and sonochemistry.

Because the bubble dynamics are altered by the inclusion of water vapour, we use the compression ratio as the distinguishing parameter. In figure 11, we plot the maximum centre temperature versus the compression ratio for cases I, II and III. The calculations in figure 11 are devoid of strong shocks, a matter to which we devote more attention below. If there are strong shocks, then figure 11 will look the same in terms of a suitably averaged temperature rather than the centre temperature.

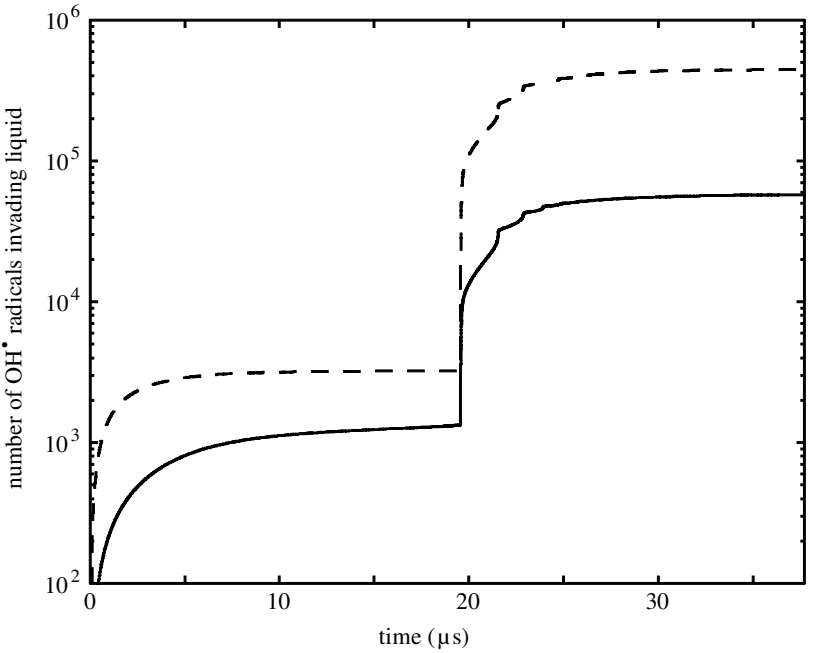

Figure 10. Comparison of the amount of $OH^{\bullet}$ absorbed by the liquid versus time for cases IV(a) (——, uptake coefficient $\Theta = 0.001$) and IV(b) (– – –, $\Theta = 0.01$). Most of the $OH^{\bullet}$ uptake occurs at the main collapse and the subsequent after-bounce.

In case I, the plot shows linear behaviour (on the log–log scale). One observes that when water vapour is not taken into account, stronger forcing yields more extreme temperatures.

In case II, the relationship between compression ratio and maximum temperature is very different. First, we note that the amount of water trapped in the bubble increases with compression ratio. If we revisit the water-trapping mechanism (§ 3 *a* (iii)), this trend is readily explained. The increase in water-vapour content reduces the ratio of specific heats of the gas–vapour mixture and, hence, reduces the compression heating.

At low compression ratios in case II, the temperature increases with compression ratio in a manner very similar to case I. At low compression ratios, the amount of water at collapse is very small; the bubble is nearly pure argon. As the forcing is increased, more water is trapped and the maximum temperature of the bubble becomes nearly constant. In this range of bubble dynamics, there is an almost perfectly compensating effect (with respect to peak temperature) between the decrease in specific-heat ratio and the increase in compression. Case III is very similar to case II, except that the plateau in temperature occurs at a lower temperature, a consequence of the endothermic chemical reactions.

(*e*) *Inclusion of water vapour promotes the formation of shocks*

Water vapour is of great importance in the formation of shocks in very strongly forced bubbles. We shall briefly consider a 6.0 μm bubble forced with a pressure amplitude of 1.4 bar at a frequency of 20.6 kHz (Case A1 in Moss *et al.* (1999)).

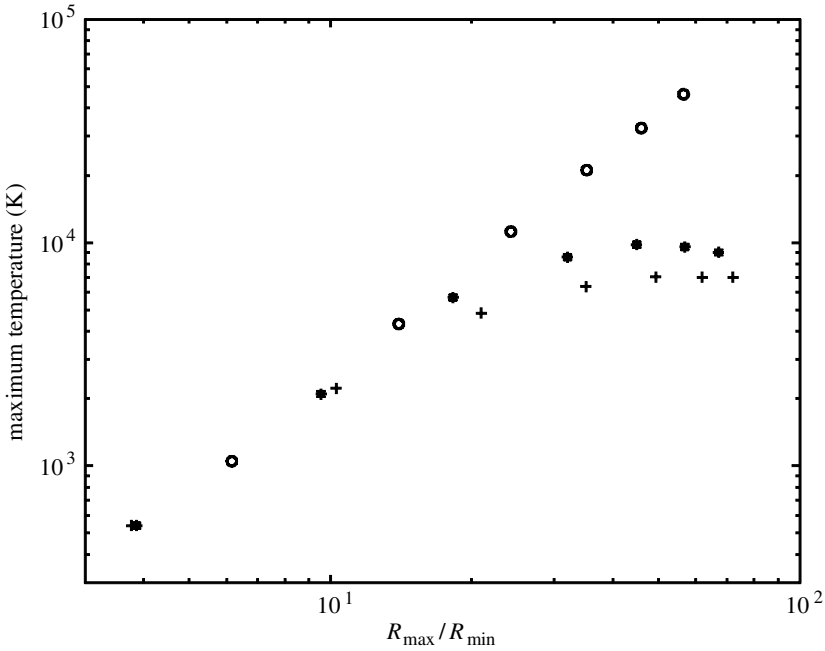

Figure 11. Change in centre temperature versus compression ratio in cases I (○), II (∗) and III (+). In this plot, all parameters were held constant except the pressure amplitude, which was varied between 1.0 and 1.3 bar. Case I shows a steady increase in temperature with compression ratio. Cases II and III reach a maximum temperature as the forcing is increased.

When water vapour is neglected, a compression wave is launched into the bubble on collapse, but the wave does not steepen into a shock. When water vapour is taken into account (with or without reactions), the compression wave steepens into a strong shock very near the centre of the bubble. Vuong *et al.* (1999) showed that the rate of steepening depends on the amount of compression heating *before* the compression wave is launched.

In very recent work, Lin & Szeri (2000) used the wavefront expansion technique to determine the evolution of a compression or rarefaction wavefront that is propagating spherically into a collapsing or expanding gas of non-uniform entropy. This analytical work supports the idea that when the speed of sound is higher at the centre (due to temperature and composition inhomogeneities), shock formation is delayed or prevented. Furthermore, this work demonstrated that the inward radial velocity also hinders the steepening of compression waves into shocks.

Consistent with the arguments made in Lin & Szeri (2000), Vuong *et al.* (1999) and Moss *et al.* (1999), our results show that the decrease in the ratio of specific heats due to an increase in the water-vapour content can promote shock formation. The point we want to emphasize is that the question of shock formation cannot be undertaken without consideration of water vapour.

With respect to total chemical production, shocks are of negligible consequence. The shock influences only about the inner 10% of the radius, which is only 0.1% of the volume. Therefore, the increased production of $OH^{\bullet}$ at the centre does not affect the total amount produced in the bubble.

4. Relevance to sonochemistry

In sonochemistry, one interpretation of how much $OH^{\bullet}$ is available to react in the liquid is to assume that, in multi-bubble situations, the bubbles will be unstable on collapse and break apart, in some way dispersing their total $OH^{\bullet}$ content into the liquid. This view was promoted by Colussi *et al.* (1998). If we take this view, we might regard the peak amount of $OH^{\bullet}$ in figure 7 to be the available sonochemical $OH^{\bullet}$. We remind the reader that peak amounts of total $OH^{\bullet}$ at the collapses are completely insensitive to the uptake coefficient.

An alternative view is that the bubbles are stable and the $OH^{\bullet}$ radicals enter the liquid by uptake across the interface. If we take this view, we might regard the amount of $OH^{\bullet}$ in figure 10 to be the available sonochemical $OH^{\bullet}$ for each cycle. The total mass of $OH^{\bullet}$ leaving the bubble depends on the concentration at the wall and on the uptake coefficient, as we have shown.

We expect that, in reality, the $OH^{\bullet}$ transport to the liquid would be some combination of these two proposed mechanisms: the important mechanism will depend upon the application. The total amount of $OH^{\bullet}$ available in the bubble is a few orders of magnitude greater than the amount taken up by the liquid in one cycle. Thus, the unstable bubble mechanism may be the important one in many applications. Bubbles would have to be stable for thousands of cycles for the mass-transfer mechanism to compete in terms of quantity of $OH^{\bullet}$ donated to the liquid. The $OH^{\bullet}$-uptake mechanism may be important in other applications.

The total amount of $OH^{\bullet}$ in the bubble is insensitive to the uptake by the liquid because the evaporation of water on every expansion provides the 'fuel' to produce many more $OH^{\bullet}$ radicals at the collapse than are lost via uptake to the liquid (assuming a stable bubble). Reactions involving O and H chemistry should be contrasted with the chemistry of other species. One example is the dissociation hypothesis of air bubbles (Lohse *et al.* 1997). The hypothesis is that on the collapse of an air bubble, the nitrogen reacts with water vapour, producing NH_3, a very soluble species. The NH_3 will tend to leave the bubble at a fast rate (i.e. the associated uptake coefficient is large). While small amounts of dissolved N_2 will come into the bubble on the next expansion when the bubble is larger than the ambient radius, this rate is slow compared with the uptake of NH_3. The bubble is soon devoid of nitrogen due to the ease with which NH_3 leaves the bubble compared with the difficulty with which N_2 enters it.

Hence, for understanding the composition of stable bubbles, $OH^{\bullet}$ uptake by the liquid is *not* important, due to rapid evaporation of H_2O on the expansion. NH_3 uptake *is* important due to the slow rate that N_2 enters the bubble on the expansion. One should keep these facts in mind when thinking of how the present results on water-vapour chemistry may apply to chemical systems more complicated than a monatomic gas and water.

Finally, on the basis of the findings presented in this paper, one might be tempted to think that simply by suppressing evaporation of water into the bubble, e.g. by adding salt or reducing the bath temperature, one has direct control over conditions at the collapse. The situation is, however, more complicated, because adding salt (Wall *et al.* 1999) or manipulating the liquid temperature can drastically change the gas solubility. The change in solubility can affect the ambient bubble radius, leading to different bubble dynamics.

5. Conclusions

In this paper we attempted to illuminate the important role that water vapour plays in the physics of strongly collapsing bubbles. Water vapour is trapped inside the bubble during the violent collapse. The amount and distribution of water vapour in the bubble is frozen on the time-scale of the peak temperature. The trapping mechanism can be understood by a relative-time-scales argument: the bubble-dynamics time-scale becomes much faster than the mass-diffusion time-scale at some point in the collapse. The amount of water left behind depends sensitively on the non-equilibrium phase change.

The trapped water vapour undergoes chemical reactions on the time-scale of the bubble dynamics. The products of reaction inside the bubble are distributed according to where chemical reactions occur; diffusion effects are small in this regard. Due to the large temperature gradient at the bubble wall, most of the chemical activity occurs within the bubble interior. This temperature gradient keeps the concentration of $OH^{\bullet}$ about three orders of magnitude lower at the wall than at the centre. Water vapour and its destruction in endothermic chemical reactions significantly reduce the peak temperatures achieved during the rapid collapse.

The phenomenon of $OH^{\bullet}$ uptake into the liquid had only a small effect on the overall properties of the bubble (i.e. mass, temperature, composition). This insensitivity to $OH^{\bullet}$ uptake into the liquid is due to the fact that the large amounts of $OH^{\bullet}$ produced by the bubble remain in the centre and the $OH^{\bullet}$ concentration at the wall remains relatively low.

Through variations of parameters we explored some interesting trends when water vapour and reactions are taken into account. When water vapour is neglected, the peak temperature achieved in the collapse increases with forcing when all other parameters are fixed. When water vapour is included, the simultaneous increase in water content and compression ratio with increased forcing nearly compensate one another: the consequence is that the peak temperature of the bubble is nearly constant with increased forcing. This is an example of an important trend that changes if water is not taken into account.

We also investigated the case of more strongly forced bubbles. We showed that neglect of water vapour can prevent shocks from forming. When water vapour is allowed into the bubble, a shock can form near the centre in very strongly forced cases. Physical phenomena can be overlooked if water vapour is neglected.

We discussed the relevance of this work to sonochemistry. Two ideas have been advanced for $OH^{\bullet}$ dispersal into the liquid. The first mechanism assumes that the bubble bursts on collapse and that the $OH^{\bullet}$ is somehow mixed with the liquid. The second mechanism assumes that the bubble is stable and that the $OH^{\bullet}$ is taken in by the liquid throughout the bubble oscillations. The second mechanism is far less productive than the first.

Finally, we finish with a connection to light emission that provides a measure of confidence in the present results. The amount of water vapour that Moss *et al.* (1999) used was determined by matching their calculated results with the experimental data for photon yields and pulse widths measured by Gaitan & Holt (1999) and Hiller *et al.* (1998), respectively. In table 2, we compare the uniform molar fraction of water vapour that Moss *et al.* (1999) used with the amount we determined with the present method. Because the composition is non-uniform, we give the fraction of vapour at

Table 2. *Comparison of the amount of water vapour trapped in the bubble at collapse determined by the present work versus the amount determined by Moss et al. (1999)*

(The vapour in Moss *et al.* (1999) was assumed to be uniform throughout the bubble. The mole fraction of vapour at the centre and based on the total contents, determined by the present method, is compared with the (uniform) fraction determined by Moss *et al.* (1999) to yield photon counts and pulse widths in concert with experiments (see text). The case number refers to table 1 in Moss *et al.* (1999).)

case	R_0 (μm)	P_A (bar)	vapour Moss (%)	vapour centre (%)	vapour total (%)
A1	6.0	1.40	40	56	33
B1	4.0	1.32	36	48	27
C1	2.1	1.29	30	41	22

the centre and based on the total bubble contents. One observes not only that the actual numbers are in excellent agreement, but that the trend is captured as well.

This research was supported by the National Science Foundation. The authors thank W. C. Moss, D. A. Young, J.-Y. Chen, M. Frenklach, J. Reisse, K. Bartik, H.-P. Schuchmann and C. Von Sonntag for useful discussions and help with references.

References

Barber, B. P., Weninger, K. & Putterman, S. J. 1997 Sonoluminescence. *Phil. Trans. R. Soc. Lond.* A **355**, 641–644.

Bird, R. B., Stewart, W. E. & Lightfoot, E. N. 1960 *Transport phenomena*. Wiley.

Bowman, C. T., Hanson, R. K., Davidson, D. F., Gardiner, W. C., Lissianski, V. Smith, G. P., Golden, D. M., Frenklach, M. & Goldenberg, M. 1999 http://www.me.berkeley.edu/gri_mech/.

Carey, V. P. 1992 *Liquid–vapor phase change phenomena*. London: Taylor & Francis.

Chameides, W. L. 1984 The photochemistry of remote marine stratiform cloud. *J. Geophys. Res.* **89**, 4739–4755.

Colussi, A. J., Weavers, L. K. & Hoffman, M. R. 1998 Chemical bubble dynamics and quantitative sonochemistry. *J. Phys. Chem.* A **102**, 6927–6934.

Eames, I. W., Marr, N. J. & Sabir, H. 1997 The evaporation coefficient of water: a review. *Int. J. Heat Mass Transfer* **40**, 2963–2973.

Fristrom, R. M. & Monchik, L. 1988 Two simple approximations to the thermal-diffusion factor and their applications to flame studies. *Comb. Flame* **71**, 89–99.

Fujikawa, S. & Teruaki, A. 1980 Effects of the non-equilibrium condensation of vapour on the pressure wave produced by the collapse of a bubble in a liquid. *J. Fluid Mech.* **97**, 481–512.

Fyrillas, M. M. & Szeri, A. J. 1994 Dissolution or growth of soluble, spherical, oscillating bubbles. *J. Fluid Mech.* **277**, 381–407.

Gaitan, D. F. & Holt, R. G. 1999 Experimental observations of bubble response and light intensity near the threshold for single bubble sonoluminescence in an air–water system. *Phys. Rev.* E **59**, 5495–5502.

Gaitan, D. F., Atchley, A. A., Lewia, S. D., Carlson, J. T., Maruyama, X. K., Moran, M. & Sweider, D. 1996 Spectra of sonoluminescence in water and glycerin–water mixtures. *Phys. Rev.* E **54**, 525–528.

Gardiner, W. C. 1984 *Combustion chemistry*. Springer.

Gong, C. & Hart, D. P. 1998 Ultrasound induced cavitation and sonochemical yields. *J. Acoust. Soc. Am.* **104**, 2675–2682.

Hanson, D. R., Burkholder, J. B., Howard, C. J., Ravishankara, A. R. 1992 Measurement of OH and HO_2 radical uptake coefficients on water and sulfuric acid surfaces. *J. Phys. Chem.* **96**, 4979–4985.

Hilgenfeldt, S., Lohse, D. & Brenner, M. P. 1996 Phase diagrams for sonoluminescing bubbles. *Phys. Fluids* **8**, 2808–2826.

Hiller, R., Putterman, S. J. & Barber, B. P. 1992 Spectrum of synchronous picosecond sonoluminescence. *Phys. Rev. Lett.* **69**, 1182–1184.

Hiller, R. A., Putterman, S. J. & Weninger, K. R. 1998 Time-resolved spectra of sonoluminescence. *Phys. Rev. Lett.* **80**, 1090–1093.

Hirschfelder, J. O., Curtiss, C. F. & Bird, R. B. 1954 *Molecular theory of gases and liquids*. Wiley.

Kamath, V., Prosperetti, A. & Egolfopoulos, F. N. 1993 A theoretical study of sonoluminescence. *J. Acoust. Soc. Am.* **94**, 248–260.

Lin, H. & Szeri, A. J. 2000 Shock formation in the presence of entropy gradients. *J. Fluid Mech.* (Submitted.)

Lohse, D., Brenner, M. P., Dupont, T. F., Hilgenfeldt, S. & Johnston B. 1997 Sonoluminescing air bubbles rectify argon. *Phys. Rev. Lett.* **78**, 1359–1362.

Maas, U. & Warnatz, J. 1988 Ignition processes in hydrogen–oxygen mixtures. *Combust. Flame* **74**, 53–69.

Mason, T. J. 1999 Sonochemistry: current uses and future prospects in the chemical and processing industries. *Phil. Trans. R. Soc. Lond.* A **357**, 355–369.

Moss, W. C., Clarke, D. B. & Young, D. A. 1997 Calculated pulse widths and spectra of a single sonoluminescence bubble. *Science* **276**, 1398–1401.

Moss, W. C., Young, D. A., Harte, J. A., Levatin, J. L., Rozsnyai, B. F., Zimmerman, G. B. & Zimmerman, I. H. 1999 Computed optical emissions from a sonoluminescing bubble. *Phys. Rev.* E **59**, 2986–2992.

Press, W. H., Teukolsky, S. A., Vetterling, W. T. & Flannery, B. P. 1988 *Numerical recipes in C*. Cambridge University Press.

Prosperetti, A. & Lezzi, A. 1986 Bubble dynamics in a compressible liquid. Part 1. First-order theory. *J. Fluid Mech.* **168**, 457–477.

Reid, R. C., Prausnitz, J. M. & Poling, B. E. 1987 *Properties of gases and liquids*. McGraw-Hill.

Sander, R. 1998 Henry's Law constants. In *NIST Chemistry WebBook* (ed. W. G. Mallard & P. J. Linstrom), NIST Standard Reference Database no. 69. Gaithersburg, MD: National Institute of Standards and Technology. http://webbook.nist.gov.

Sochard, S., Wilhelm, A. M. & Delmas, H. 1997 Modeling of free radicals production in a collapsing gas-vapour bubble. *Ultrason. Sonochem.* **4**, 77–84.

Storey, B. D. & Szeri, A. J. 1999 Mixture segregation within sonoluminescence bubbles. *J. Fluid Mech.* **396**, 203–221.

Suslick, K. S., Didenko, Y., Fang, M. F., Hyeon, T., Kolbeck, K. J., McNamara, W. B., Mdleleni, M. M. & Wong, M. 1999 Acoustic cavitation and its chemical consequences. *Phil. Trans. R. Soc. Lond.* A **357**, 335–353.

Takami, A., Kato, S., Shimono, A. & Seichiro, K. 1998 Uptake coefficient of OH radical on aqueous surface. *Chem. Phys.* **231**, 215–227.

Von Sonntag, C., Mark, G., Tauber, A. & Schuchmann, H.-P. 1999 OH radical formation and dosimetry in the sonolysis of aqueous solutions. *Adv. Sonochem.* **5**, 109–145.

Vuong, V. Q. & Szeri, A. J. 1996 Sonoluminescence and diffusive transport. *Phys. Fluids* **8**, 2354–2364.

Vuong, V. Q., Szeri, A. J. & Young, D. A. 1999 Shock formation within sonoluminescence bubbles. *Phys. Fluids* **11**, 10–17.

Wall, M., Ashokkumar, M., Tronson, R. & Grieser, F. 1999 Multibubble sonoluminescence in aqueous salt solutions. *Ultrason. Sonochem.* **6**, 7–14.

Wu, C. C. & Roberts, P. H. 1998*a* Bubble shape instability and sonoluminescence. *Phys. Lett.* A **250**, 131–136.

Wu, C. C. & Roberts, P. H. 1998*b* On rectified diffusion and sonoluminescence. *Theor. Comput. Fluid Dynam.* **10**, 357–372.

Yasui, K. 1997*a* Alternative model of single-bubble sonoluminescence. *Phys. Rev.* E **56**, 6750–6760.

Yasui, K. 1997*b* Chemical reactions in a sonoluminescing bubble. *J. Phys. Soc. Japan* **66**, 2911–2920.